Ab initio derivation of flavin hyperfine interactions for the protein magnetosensor cryptochrome

Jean Deviers, Fabien Cailliez, Bernardo Zúñiga Gutiérrez, Daniel Kattnig, Aurélien de la Lande

Ab initio derivation of flavin hyperfine interactions for the protein magnetosensor cryptochrome

Jean Deviers[1,2], Fabien Cailliez[2], Bernardo Zúñiga Gutiérrez[3], Daniel R. Kattnig[1], and Aurélien de la Lande[2]

[1]Living Systems Institute and Department of Physics, University of Exeter, Stocker Road, Exeter, Devon, EX4 4QD, United Kingdom
[2]Institut de Chimie Physique, CNRS UMR 8000, Université Paris-Saclay, 91405 Orsay, France
[3]Departamento de Química, Universidad de Guadalajara, Blvd. Marcelino García Barragán 1421, C. P. 44430, Guadalajara Jal, Mexico

Abstract

The radicals derived from flavin adenine dinucleotide (FAD) are a corner stone of recent hypotheses about magnetoreception, including the compass of migratory songbirds. These models attribute a magnetic sense to coherent spin dynamics in radical pairs within the flavo-protein cryptochrome. The primary determinant of sensitivity and directionality of this process are the hyperfine interactions of the involved radicals. Here, we present a comprehensive computational study of the hyperfine couplings in the protonated and unprotonated FAD radicals in cryptochrome 4 from *C. livia*. We combine long 800 ns molecular dynamics trajectories to accurate quantum chemistry calculations. Hyperfine parameters are derived using auxiliary density functional theory applied to cluster and hybrid QM/MM (Quantum Mechanics/Molecular Mechanics) models comprising the FAD and its significant surrounding environment, as determined by a detailed sensitivity analysis. Thanks to this protocol we elucidate the sensitivity of the hyperfine interaction parameters to structural fluctuations and the polarisation effect of the protein environment. We find that the ensemble-averaged hyperfine interactions are predominantly governed by thermally induced geometric distortions of the flavin. We discuss our results in view of the expected performance of these radicals as part of a magnetoreceptor. Our data could be used to parametrize spin Hamiltonians including not only average values but also standard deviations.

1 Introduction

Magnetoreception is widespread in the animal kingdom.[1] Despite the phenomenon being well established, the sensory mechanism–and even the underlying principle–has remained opaque for decades.[2] In birds and a few other species, a compass sense has been attributed to a radical pair recombination reaction in the protein cryptochrome.[3–5] This spin-selective reaction acquires magnetosensitivity, because the electron spin states of the radical pair coherently interconvert between singlet and triplet states, as the electron spins couple to the applied and

local magnetic fields. The latter are caused by the magnetic moments of nuclear spins in the radicals, *i.e.* arise via hyperfine interactions. In this way, hyperfine couplings, including the isotropic Fermi contact and the anisotropic dipole-dipole contributions, are critical in determining the magnetosensitivity and its directionality in the geomagnetic field, which governs the sensitivity of the compass.

The concept of a radical pair model of magnetoreception was originally suggested by Schulten *et al.*.[4] Later, Ritz *et al.* suggested the flavo-protein cryptochrome in the animals' eyes as the actual host of the magnetosensitive radical recombination process.[5] This proposition has since been supported by ample theoretical insight and biological evidence.[3,6,7] Indeed, there is now a wealth of behavioural studies which confirm the existence of a light-dependent inclination compass, which can be scrambled by radio-frequency electromagnetic fields, as expected for the radical pair model.[3] However, the details of the sensor and its associated pathways have remained elusive so far.

Cryptochromes contain a non-covalently bound flavin adenine dinucleotide (FAD) cofactor, which is tightly linked to its function as a magnetosensor.[8] This flavin exists in two important radical forms, the anion radical ($FAD^{\bullet -}$) and its protonated semiquinone form ($FADH^{\bullet}$), which both have been implicated as members of the magnetosensitive radical pair intermediate. The photo-reduction of fully oxidised flavin in the cryptochrome gives rise to a radical pair, comprising the $FAD^{\bullet -}$ and a surface-exposed tryptophan radical cation, which has been found to be magnetosensitive *in vitro* in the isolated protein, albeit at magnetic fields significantly exceeding the geomagnetic field.[9] $FADH^{\bullet}$ can result from protonation of the anion radical or oxidation of the fully reduced flavin cofactor, $FADH^{-}$. The latter reaction has been suggested to underpin magnetoreception in the dark.[10–14] While there is ongoing debate about the identity[15–17] of the partner radical and even the number[18–22] of radicals involved, the flavin radical, either protonated or in is anionic form, is a central cornerstone of all models.

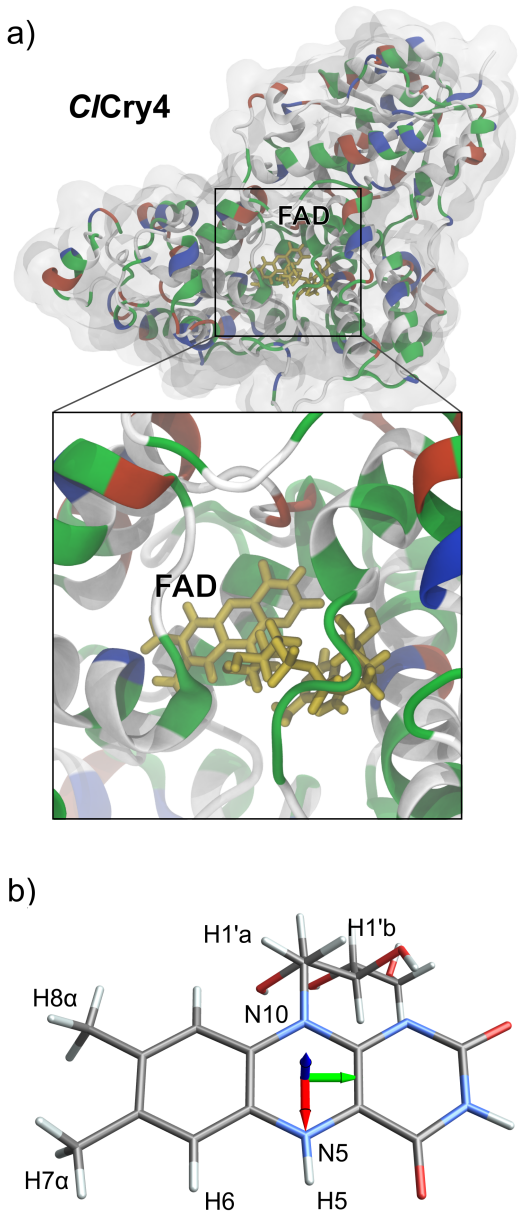

Figure 1: Graphical representation of (a) the pigeon cryptochrome 4 protein (*Cl*Cry4; PDB ID: 6PU0 with phosphate binding loop reconstructed) and (b) the FAD cofactor in its semiquinone form $FADH^{\bullet}$. (a) shows the chemical environment of the flavin. Residues coloured in blue are cationic; in red, anionic; and in green, polar. (b) introduces the numbering scheme for pertinent nuclei and the standard orientation used throughout this paper. Red axis = $\mathbf{x}$, green = $\mathbf{y}$, blue = $\mathbf{z}$. In the anion radical $FAD^{\bullet-}$, the hydrogen labeled H5 is absent. H7α and H8α are generic labels for the 3 hydrogens born by the methyl groups on the isoalloxazine ring.

The hyperfine interaction parameters in the involved radicals are crucial in determining the directional sensitivity of the compass. The hyperfine couplings (HFCs) of the flavin

radicals are generally perceived as ideal for its putative function in a directional sensor.[3,16,23] This is the result of the hyperfine structure being dominated by the HFCs of the two central nitrogen atoms of the isoalloxazine ring system, N5 and N10 (see Fig. 1), which are strongly anisotropic, close to axial and collinear. In the absence of other strong HFCs, this gives a dominant directionality to the spin dynamics.[16] Particularly large anisotropic magnetic field effects in the geomagnetic field result if these flavin radicals are combined with radicals devoid of hyperfine interactions, *i.e.* in so-called reference-probe configurations.[16,24] On the other hand, partner radicals without overarching symmetry of their hyperfine couplings strongly attenuate magnetic fields effects.[17,23]

Interestingly, the hyperfine structure can impact the spin dynamics in a non-obvious way too: in combination with anisotropic hyperfine interactions in the partner radical (e.g. as provided by a protein-bound tryptophan radical), the flavin anion HFC structure can give rise to a spike in the recombination yield of long-lived radical pairs, which results from a level anti-crossing phenomenon when the magnetic field is parallel to the isoalloxazine ring plane.[23] This remarkable observation emphasizes the truly quantum nature of cryptochrome magnetoreception, as the feature is only apparent in fully quantum spin dynamics simulations, but absent in semi-classical realisations of the modeling.[25] The effect too relies on the hyperfine interactions of N5 and N10, specifically on the small but, importantly, nonzero transverse components. A small increase in their magnitude has been shown to enhance the effect.[23]

Many theoretical studies have been dedicated to understanding the electronic structure and properties of flavins in proteins. The reader is referred to Kar *et al.* for a review focusing on electronic spectra.[26] On the other hand, theoretical studies aiming to calculate hyperfine tensors for flavin radicals are much fewer, and either neglect dynamical effects,[27] include the environment using an implicit solvent model,[28] approximate the flavin by a truncated analogue,[23,29] or work on proteins not implicated in avian magnetoreception. Indeed, hyperfine interactions and g-matrices have only been predicted for the bound flavin radicals in glucose oxidase from *A. niger*, whereby a QM/MM molecular modeling approach was chosen.[30] The authors' conclusion, that incorporation of at least the nearest protein environment of the cofactor radicals proved to be vital for a correct reproduction of shifts in g-matrix components, supports the idea that accurate coupling parameters for the simulation of the avian magnetic compass must be computed in an avian protein, as we do here. Note however that the MD simulations reported in ref. 30 were based from short MD simulations of only 10 ps. Extensive exploration of the coupling parameters over long simulations are thus needed and will be reported in this article.

Similarly, the hyperfine interactions in the flavin radicals are expected to be sensitive to their protein environment; the HFCs can for example be modulated by substrate binding, altered geometries of hydrogen bonds, or the surrounding amino acids, as has been shown experimentally[31–37] and theoretically.[30,38–40] In addition to these static environmental effects, hyperfine interactions are dynamically modulated due to the thermal motions of the radicals in the protein–an unavoidable consequence of "warm, wet and noisy" biological environments. If the hyperfine interactions are modulated on a timescale fast relative to the timescale of spin evolution, this induced noise in the hyperfine parameters give rise to spin relaxation.[41] If, on the other hand, the modulation is slow, the magnetosensitive response is that of an inhomogeneous ensemble rather than that of a single radical pair. Procopio and Ritz have investigated the performance of the compass in response to such inhomogeneities in the hyperfine parameters and found that the choice of radical pair hyperfine parameters

greatly influences the directional sensitivity.[39]

Despite the critical importance of the hyperfine parameters of flavin in the cryptochrome for assessing the radical pair hypothesis, little is actually known about them. Electron paramagnetic resonance (EPR) spectroscopy can reveal some of the hyperfine parameters of flavin radicals in cryptochromes and remotely related flavo-enzymes, such as Light, Oxygen, or Voltage sensing (LOV) and Blue-Light-Utilizing flavin adenine dinucleotide (BLUF) domains.[42,43] Conventional EPR spectroscopy, in particular if carried out at high frequencies, allows measuring some components of the anisotropic HFCs of N5, N10, and H5. ENDOR spectroscopy shows the fingerprints of H5, H6, the protons of the methyl group at C8, *i.e.* H8α, and often one of the two β-protons attached to C1'. Time-resolved EPR can reveal a few HFCs of flavins in members of radical pairs.[44] While particular components of selected nuclei are thus accessible spectroscopically, the interactions of weakly coupled nuclei and the principal orientations are currently only inferable from computational approaches.

Many previous theoretical studies of spin dynamics in cryptochrome have relied on hyperfine tensors calculated on an isolated lumiflavin, ignoring environmental effects. Recently, the crystal structure of cryptochrome 4 (*Cl*Cry4) of *Columba livia* (PDB ID: 6PU0) has been resolved (for a large part of the protein), which now, for the first time, provides the prospect of assessing the flavin hyperfine interactions in the environment of an avian cryptochrome.[45] Here, we derive hyperfine interaction parameters for the most relevant spin-bearing atoms on $FAD^{\bullet-}$ and $FADH^{\bullet}$ in *Cl*Cry4 using Auxiliary Density Functional Theory (DFT).[46–49] We employ a cluster model that considers the flavin and its immediately surrounding amino acids in the quantum region; as well as a QM/MM scheme ($MD_{QM/MM}$), for which the flavin and the side-chains of the cluster residues are kept in the quantum region while the rest of the protein environment is included as a set of point charges. We therefore reach in both models a more accurate description of polarizing environment of the flavin radical than previously described in the literature, therefore leading to more realistic HFCC evaluations. We sample conformational ensemble using long-time scale classical dynamics trajectory (800 ns) whereby snapshots are extracted at representative time intervals. This allowed us to provide accurate hyperfine coupling parameter fluctuations for an avian cryptochrome, which will inform future, more realistic spin dynamics simulations. The results of the cluster and QM/MM approaches are compared.

2 Simulation setup and computational details

2.1 Initial protein structure

Our model is based on the X-ray diffraction-resolved structure of *Columba livia* cryptochrome 4 (*Cl*Cry4, PDB ID: 6PU0).[45] The unresolved segment of the protein (residues 228-244) was reconstructed as described in ref. (50). The protonation state of aminoacid residues was assigned with the use of multiple pK_a-predictors (Yasara,[51,52] DelPhiPka,[53–55] pdb2pqr[56,57]) and ambiguous cases were resolved through visual inspection of the hydrogen-bonding pattern at the site in question. Finally, the histidine residues with index 3, 7 and 54 were found to be positively charged and doubly protonated at physiological pH (AMBER residue name: HIP); histidine residues 64, 353, 405 and 471 were neutral and singly protonated at the ε-site (HIE); all 13 remaining histidine residues were assigned as neutral and protonated at the δ-position (HID). A representative protein conformation is provided in the Supplementary Information

(SI).

2.2 MD simulations

We carried out molecular Dynamics (MD) simulations using the Amber 18 package with the ff14SB force field for the protein; the flavin radicals $FAD^{\bullet -}$ and $FADH^{\bullet}$ were modeled based on previously established RESP atomic charges.[58,59] The TIP3P model was used for water molecules. Cl^- was added to neutralise the system; additional Na^+ and Cl^- ions were used to realize a NaCl concentration of 50 mM. A standard series of energy minimisation, heating and equilibration steps was then applied, following the protocol in Fox *et al.*,[60] in order to allow the system to relax and stabilise its density to $1.006\,\mathrm{g\,cm^{-3}}$, for box dimensions of approximately $90 \times 92 \times 102\,\mathrm{Å}^3$.

The production run for the solvated protein/flavin complex was performed in the NVT ensemble and spanned 800 ns for each protonation state of FAD, with $T = 313\,\mathrm{K}$ and a time step of 2 fs. A Langevin thermostat was employed to maintain the temperature, and the SHAKE algorithm was used to constrain the length of hydrogen bonds.[61,62] A cutoff of 9.0 Å was applied for non-bonded interactions.

2.3 DFT calculations

Magnetic properties were calculated using auxiliary-density-functional theory (aDFT) as implemented in deMon2k.[63] aDFT makes use of variationally fitted electronic densities to speed-up the calculation of classical electronic repulsion and exchange-correction (XC) contributions, including exact exchange.[64] The details of the aDFT methodology to compute HFC tensors will be published elsewhere. The calculated tensors include Fermi contact, spin-dipole and paramagnetic spin orbit-spin orbit coupling contributions. We tested and benchmarked the calculation of HFC tensors testing various basis sets (more details presented in SI and discussed below).

It transpired from our tests that an accurate evaluation of HFC tensors involving flavin nuclei requires a detailed description of the electron density on the flavin and a adequate representation of the surrounding electron density. We also tested a mixed basis set scheme for the flavin, where a high-precision basis set is used on magnetic nuclei and a cheaper one for the other atoms. It emerged that using such a scheme, as opposed to the "full basis" approach where the high precision basis set is applied on all flavin atoms, allows a significant speed-up at a moderate accuracy cost (see figures S2 and S3 of the SI). We thus selected for the flavin atoms the combination of EPR-III/GEN-A2* atomic orbitals and auxiliary basis sets for magnetic nuclei, and a combination of DZVP-GGA/GEN-A2 basis functions for the remaining flavin atoms and the close environment. We chose the B3LYP (Becke, Lee, Yang and Parr) XC functional[65–67] based on previous studies showing its suitability for evaluating HFC tensors with good accuracy.[68] An adaptive grid ensuring an accuracy of $10^{-6}\,\mathrm{Ha}$ on the diagonal elements of the XC matrix was used.[69] The unrestricted Kohn-Sham formalism was chosen as the SCF procedure. A dynamic level shifting of 0.1 Ha was applied to facilitate convergence.

Inclusion of the full protein environment with a QM/MM scheme: To complement the cluster approach outlined in the previous paragraph, we also set up a QM/MM partitioning

scheme, whereby the truncated flavin *and* the "minimal cluster" are explicitly included in the subsequent DFT calculation to compute hyperfine coupling tensors on the flavin, while all the other atoms in the system–*i.e* the ribityl and adenosine moieties of the flavin, the backbone atoms of the "minimal cluster" residues, all other residues in the protein, water molecules and ions– are included as point charges that polarise the distribution of electronic density of the QM region. These point charges were the same as those used in the MD simulations to generate the trajectories. The additive QM/MM methodology we chose was described in detail in Ref. [70].

Note that the delineated QM/MM approach does not constitute an incremental increase in the quality of the description over the cluster approach described above, for which the minimal cluster is directly subject to the DFT calculation of HFC tensors. This is the consequence of the standard methodology for partitioning proteins into QM and MM parts, which mandates to only include side-chains, and not the backbone atoms, into the QM framework. The rational for this is that in a QM/MM scheme, a "link atom" is inserted at the point where the cut is made, to avoid nonphysical dangling bonds by saturating the valence of the QM region. If the cut were done, as in the cluster scheme from above, at the backbone C-N bond between the amino group and the next residue's carboxyl group, then the link atom would be inserted on the N atom and along the axis of this cut N-C bond, yielding a terminating amine with a sp^2 nitrogen instead of a properly pyramidalised sp^3. This strained geometry of the QM region makes it extremely difficult to converge the DFT calculations. Besides, a more realistic model is obtained when cutting and protonating an apolar bond rather than a polar one.

2.4 Metrics

We consider in this work various parameters to quantify HFC tensors. Let A_{11}, A_{22} and A_{33} be the eigenvalues of the HFC tensor. We refer to the isotropic HFC as

$$a_{iso} = \frac{(A_{11} + A_{22} + A_{33})}{3} \tag{1}$$

We order the principal components, A_{11}, A_{22} and A_{33}, according to their separation from the isotropic value (Haeberlen convention). That is, we assign $\{A_{11}, A_{22}, A_{33}\}$ to the labels $\{A_{xx}, A_{yy}, A_{zz}\}$ such that

$$|A_{zz} - a_{iso}| \geq |A_{xx} - a_{iso}| \geq |A_{yy} - a_{iso}|, \tag{2}$$

i.e. A_{xx}, A_{yy}, A_{zz} are a permutation of A_{11}, A_{22}, A_{33}. We then define the anisotropy and the asymmetry of HFC tensors as

$$\Delta A = A_{zz} - \frac{A_{xx} + A_{yy}}{2} = \frac{3}{2}(A_{zz} - a_{iso}) \text{ and} \tag{3}$$

$$\eta = \frac{A_{yy} - A_{xx}}{A_{zz} - a_{iso}}, \tag{4}$$

respectively. These parameters are independent of the coordinate system used.

The uncertainty on the mean of HFC tensors' eigenvalues is computed as follows:

$$U(A_{ii}) = \frac{t \times s}{\sqrt{N_{eff}}}$$

where t is the Student's t-factor – here, $t = 1.96$ for a confidence level of 95.5% –, s is the standard deviation of the sample and N_{eff} is the effective size of this sample, computed using the R function `coda::effectiveSize(x)`.[71,72] `coda::effectiveSize(x)` computes $N_{\text{eff}} = N \times \frac{\lambda^2}{\sigma^2}$, where λ^2 is the sample variance and σ^2 is an estimate of the spectral density at frequency zero.

Following the rules of combination of uncertainties, we calculate the uncertainty of the mean a_{iso} using:

$$U(a_{\text{iso}}) = \frac{U(A_{\text{yy}}) + U(A_{\text{zz}}) + U(A_{\text{zz}})}{3}$$

and on the mean of ΔA using:

$$U(\Delta A) = U(\text{A}_{\text{zz}}) + \frac{U(\text{A}_{\text{xx}}) + U(\text{A}_{\text{yy}})}{2}$$

3 Results

We have aimed to sample the dynamic heterogeneity of hyperfine coupling parameters of the flavin radicals bound in a representative cryptochrome. To this end, we have run extensive MD simulations of $\text{FAD}^{\bullet-}$ and $\text{FADH}^{\bullet}$ in *Cl*Cry4, as described in the "Simulation setup and computational details" section. For both $\text{FAD}^{\bullet-}$ and $\text{FADH}^{\bullet}$, we extracted 400 geometries, evenly spaced by 2 ns across the entire length of the 800 ns MD trajectories.

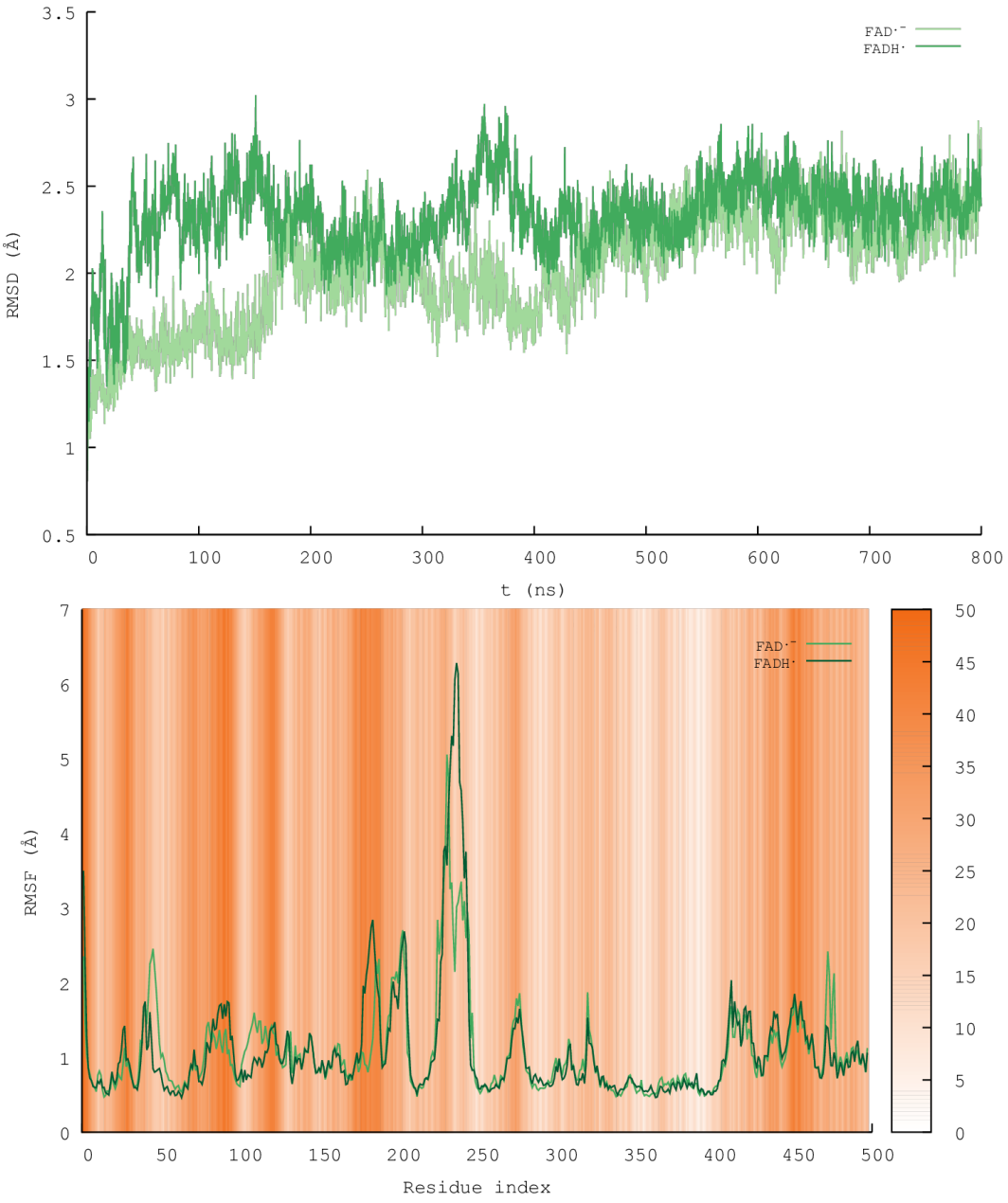

Figure 2: Various geometrical markers of the flavin-binding 6PU0 protein along a 800-ns MD trajectory in the two protonation states of the flavin radical ($FAD^{\bullet -}$ in light green and $FADH^{\bullet}$ in dark green): (top) RMSD of the backbone atoms; (bottom) RMSF of each residue's CA (backbone) atom, with distance to the center-of-mass of the flavin (in $\mathring{A}$) represented by background colour.

Validation of the Molecular Dynamics simulations: Figure 2 (top) reports the Root-Mean-Square Deviations (RMSD) of the positions of the protein backbone atoms (CA, C, O, N in the AMBER naming convention) along a 800 ns MD trajectory of solvated 6PU0 protein containing either the $FADH^{\bullet}$ or the $FAD^{\bullet -}$ flavin cofactor. This metric, along with

visual examination of the protein structure along the trajectory, reveals a preserved secondary structure throughout the simulation. Figure 2 (bottom) offers with the RMSF (Root-Mean-Square Fluctuations) a time-averaged, residue-disaggregated view which allows to identify the mobile regions of the protein. For both protonation states of the flavin the most flexible section of the backbone corresponds to the unresolved and reconstructed loop (residues 228 to 244), in agreement with Ref. 50. The background colour of Fig. 2 (bottom) indicates the distance between the centre of masses (COM) of the residue in question and the isoalloxazine moiety of the flavin. We note that the residues closest to the flavin (visible as pale bands), *i.e* those that constitute its chemical environment, are mostly residues with low RMSF. This suggests the immediate chemical environment of the flavin remains comparably constant throughout the simulation, although this claim can here only be made for the backbone atoms and not the side-chains.

A hydrogen-bonding analysis, performed using the `Cpptraj`[73] software on purely geometrical criteria, revealed no H-bonding involving the flavin isoalloxazine moiety as either a donor or acceptor, which has implications for its magnetic properties; indeed, it was shown that H-bonding to the isoalloxazine perturbs the spin density distribution in this area.[32] Water molecules infrequently enter the flavin binding cavity, and when they do, typically hover closer to the ribityl chain atoms than to the isoalloxazine. Counter-ions, namely Na^+ and Cl^-, were never found within $10\mathring{A}$ of the isoalloxazine.

Another geometrical marker relevant in the context of magnetoreception that was tracked along the trajectory is the inter-residue distance in the electron-transfer (ET) chain. This is reported in Fig. S1 (a) and (b), and we note that these distances remain stable throughout both simulations. This is expected to ensure the efficient and reliable formation of a flavin - tryptophan or flavin - tyrosine radical pairs, both of which have been proposed as agents in magnetosensitive reactions schemes.

Before conducting extensive HFC tensor calculations on structures sampled from the MD trajectories, we validated our sampling protocol and benchmarked the quantum chemistry method to be used.

Validation of the HFC calculation method: A multitude of XC functionals have been suggested for calculating hyperfine coupling parameters. The B3LYP functional in combination with the EPR-II or EPR-III basis set, from the Barone group,[74] is well established.[75–77] Jakobsen and Jensen[77] have recently suggested a series of double-ζ to pentuple-ζ polarisation-consistent basis sets with additional tight functions optimised for the calculation of hyperfine interactions, named pcH-ζ. In addition, we have also considered the B3LYP/N07D scheme, likewise proposed by Barone and coworkers,[76] which has been found remarkably accurate for a large set of radicals whilst being computationally cheap. Comparing the runtimes and isotropic hyperfine couplings parameters for a $FADH^\bullet$ relaxed in vacuum (Figure S2**a** in the SI), we find that, for our application, B3LYP/EPR-III offers the best compromise between accuracy (assessed relative to pcH-3, the most expensive basis set tried) and computational effort. A further speed-up could be achieved with the use of the "mixed basis set" approach, in which the EPR-III basis set is only applied on the atoms for which magnetic properties are calculated, while a double-ζ basis set is used for the rest of the flavin. Figure S3 in the SI shows the magnitude of the error associated with this approximation. We further confirmed that the aDFT framework did not introduce artefacts in the calculation of HFC tensors (see Table S2 in the SI) and have thus decided to use this approach for the rest of the study.

Delineation of a minimal chemical environment for the flavin: Having validated the classical MD approach and chosen a suitable method for calculating hyperfine coupling tensors, we next set out to explore electronic and steric effects of the protein environment on the hyperfine couplings of the flavin. A possible strategy would be to rely on a hybrid QM/MM methodology in which the flavin would be described at the quantum mechanical level while the environment (protein or solvent) would be described by MM point charges. Repeating such QM/MM calculations along a classical MD simulation would then provide distributions of HFCC. In the study of flavin bound in glucose oxidase from Pauwles et al, the QM regions was for example restricted to a lumiflavin fragment. This MD+QM/MM strategy enforces spin localization on the flavin moieties, and assumes that electron density polarization is adequately captured by sets of point charges. For *C. livia* cryptochrome, our calculations indicate that spin density largely localize on flavin, (see Table S5 in the SI). However, due to the presence of both polar and apolar, charged and neutral residues (see Fig. 1), individual residues may have variable effects on the distribution of electronic/spin density on the flavin. Therefore, we aim in this work to reach an accurate electrostatic embedding by including in the QM region not only the flavin but also the closest residues and to investigate HFCC fluctuations along long (800 ns) MD simulations. To select a list of amino acid residues to be described at the DFT level, we analysed 10 configurations from the MD trajectories, separated by time intervals of 20 ns.

For each snapshot, the following procedure was applied: first, all residues within 5 Å of the isoalloxazine moiety were extracted from the MD trajectory. Residues were truncated at the backbone atoms (*i.e.* cut between the carboxyl and amino groups) and hydrogen atoms were added to complete the unsaturated valences. The resulting 5-Å cluster consisted of 331 atoms in addition to the flavin, and is expected to provide a good approximation of the cofactor's steric and electronic environment. However, treating such a large number of atoms proves computationally demanding, considering that we seek to evaluate the average over long trajectories. Specifically, it was expected that selected residues could safely be removed from this cluster, thereby reducing its size and decreasing the computation effort at a marginal cost in accuracy.

In order to build such a "minimal cluster", residues were selected as follows: the individual polarising impact of each residue was measured by first computing the HFC tensors of atoms of interest for the isolated flavin in vacuum, and comparing them with the same tensors computed with this neighbouring residue explicitly included. Residues involved in a salt bridge or strong hydrogen bond were included with their counterparts: in these cases, instead of a pair, a triad (flavin - D385 - R356), or even a tetrad of molecular fragments (flavin - D387 - Y295 - R291, where hydrogen bonding also occurs with salt-bridging charged atoms) were considered at once. In order to compare the hyperfine tensors, the isotropic HFC constant, a_{iso}, and the tensor anisotropy, ΔA, were computed for the pertinent atoms on the flavin (see Fig. 1). Polarising residues were identified as those that induced a variation ($\Delta a^i_{\mathrm{iso}}$ or $\Delta\Delta A^i$) greater than one standard deviation above or below the average deviation (over all 10 selected conformers) for any considered atom i.

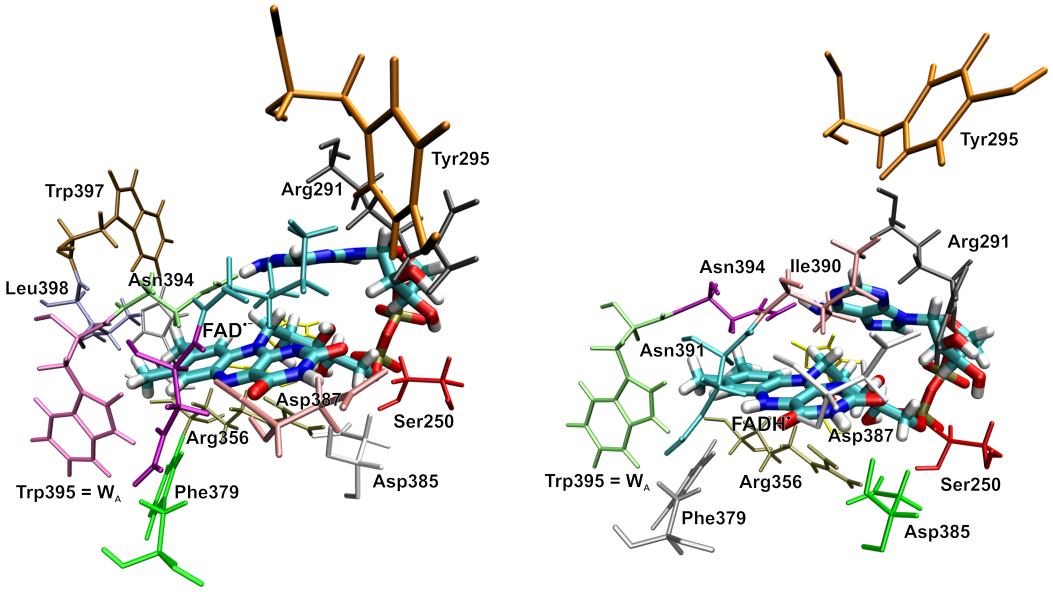

Figure 3: Graphical representation of the "minimal clusters" for $FAD^{\bullet -}$ (left) and $FADH^{\bullet}$ (right).

The final clusters so determined, shown in Figure 3, contained 272 atoms for $FADH^{\bullet}$ (S250, R291, Y295, H353, R356, F379, D385, D387, I390, N391, N394, W395, $FADH^{\bullet}$) and 333 atoms for $FAD^{\bullet -}$ (S250, R291, Y295, H353, R356, H357, F379, D385, D387, I390, N391, N394, W395, W397, L398, $FAD^{\bullet -}$). Finally, the validity of the approach was once again verified by comparing flavin-borne HFC tensors calculated in the minimal cluster with those derived for the complete cluster (Tables S3 and S4 in SI). Δa_{iso} and $\Delta\Delta A$ for $FADH^{\bullet}$ and for $FAD^{\bullet -}$ are small in magnitude and typically do not exceed 2% of the corresponding quantity. The exception is H7α on $FADH^{\bullet}$, whose very small a_{iso} value makes the relative error comparatively large. However, such a small HFC has a correspondingly minuscule impact on the spin dynamics of a magnetosensor and therefore did not warrant increasing the cluster size.

Calculation of flavin HFC tensors: With the methodology validated and the minimal representative cluster established, we set out to assess the inhomogeneity of hyperfine interactions induced by the protein environment by sampling the representative set of geometries from the long-time MD trajectories. Hyperfine coupling tensors were calculated for 400 representative geometries of the flavin in its cluster, as determined above, extracted from the MD simulations at intervals of 2 ns using deMon2k. This interval was selected to exceed the (short-time) autocorrelations of the isotropic HFC constants, thereby permitting to compute reliable statistical quantities from an unbiased sample (Table S5 in SI). We can verify with Figure S4 (in the SI) that the conformational space explored by the flavin over this length of time is representative of the entire trajectory. MD-generated geometries were rotated and aligned to the flavin molecular axis system (as represented in Figure 1b and chosen in consistency with previous spin dynamics studies).[17] This procedure also implies that the fluctuations of hyperfine couplings reported here reflect variations of the polarising environment and of the

conformation of the flavin itself, and not the librational motions of the flavin in its binding pocket, which is a source of spin relaxation.[41] Averaging the set of hyperfine interactions so obtained, a representative prediction of hyperfine interactions of the flavin in the protein environment has been realized. We report hyperfine coupling tensors for the relevant flavin atoms, for both the radical semiquinone ($FADH^{\bullet}$) and radical anion ($FAD^{\bullet -}$), in the SI. The principal components of these average hyperfine coupling tensors are reported in Table 2.

Decorrelation of structural and polarisation effects: For comparison, we also calculated a similar set of hyperfine coupling tensors from the extracted flavin geometries, without the surrounding cluster. In doing so, we aimed to quantify the electronic polarising effect of the environment, relative to the influence of structural fluctuations within the flavin. Figure 4 shows this structural variability for 80 snapshots from the extracted sample after alignment. The root-mean-square distance within these sets, calculated on the heavy atoms of the isoalloxazine moiety, is equal to 0.369 Å for $FADH^{\bullet}$ and 0.137 Å for $FAD^{\bullet -}$.

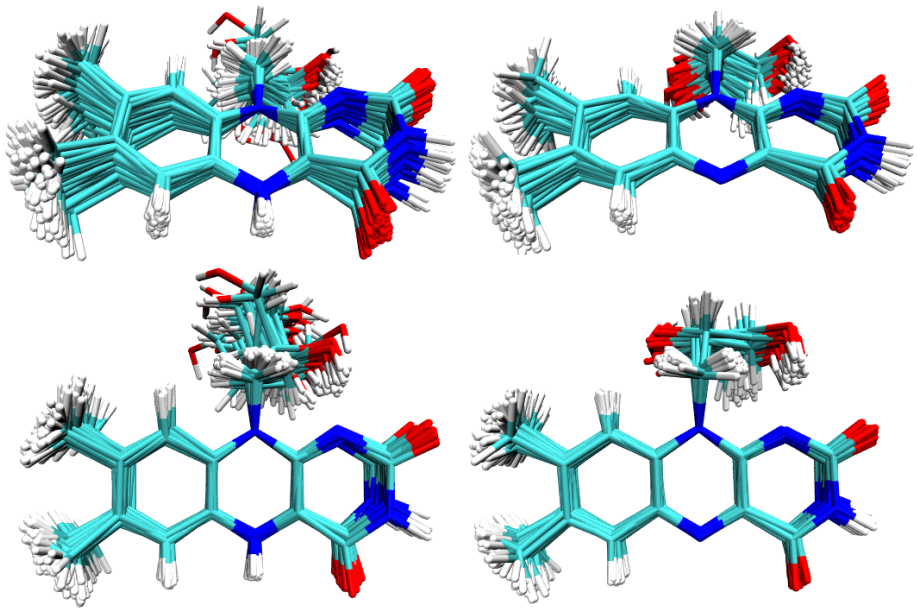

Figure 4: Flavin structural fluctuations during the MD simulations, represented by the superposition of 80 snapshots extracted from the trajectories for $FADH^{\bullet}$ (left) and $FAD^{\bullet -}$ (right).

Figure 5 is a graphical representation of average HFC tensors of $FADH^{\bullet}$ and $FAD^{\bullet -}$. To this end, we represented the hyperfine tensors by surfaces which, for direction $\mathbf{r}$, are at a distance from the nucleus proportional to $\mathbf{r^T A r}$. These graphical representations are scaled identically, making them directly comparable. In a similar way, we evaluated the standard deviation, taking the covariance of all tensor components into account. As can be seen, the hyperfine structure is generally dominated by the hyperfine constant of N5 and, for the semiquinone form, H5. The hyperfine interactions of the hydrogens of the methyl groups, (H7α and H8α on figure 1b), are averaged over the methyl group rotation: for this reason, a single effective parameter is reported throughout the paper for these groups. The largest

variance is seen for the H8α protons and, for the semiquinone form, for H5.

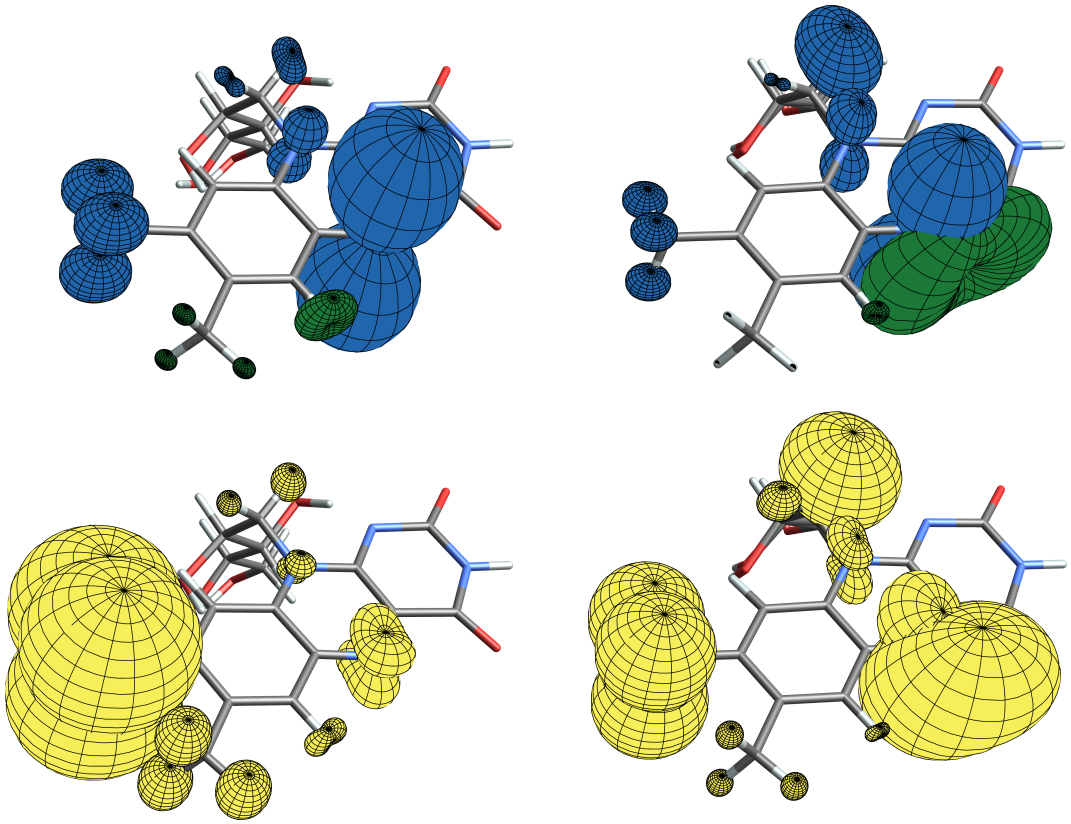

Figure 5: Graphical representation of average (top; blue/green surfaces) hyperfine coupling tensors and the standard deviation (bottom; yellow surfaces) for $FAD^{\bullet -}$ (left) and $FADH^{\bullet}$ (right), calculated using aDFT on MD-generated geometries within a "minimal" chemical environment.

The environment changes the shape and magnitude of hyperfine interactions. As can be seen in Figure S8 in the SI, which resembles Fig. 5, on the scale of these plots, these changes appear subtle. The effect is there most clearly seen for H5 and N5, which is a simple consequence of their sheer size relative to other hyperfine couplings. A better quantitative appreciation of the environment effects can be obtained from Table 2, which reports the principal components of the averaged HFC tensors, with and without the environment. Table 1 provides the associated isotropic coupling constants and anisotropies in addition to a comparison with HFC parameters calculated on the relaxed structure (obtained using PBEh-3c, as implemented in Orca[78,79]) *in vacuum*. The statistical uncertainties associated with these calculated averages are reported in Table S10 of the SI.

Table 1: Isotropic HFC and tensor anisotropy calculated using aDFT for (**a**) $FAD^{\bullet -}$ and (**b**) $FADH^{\bullet}$. The "Opt_{vac}" datasets were calculated on a single flavin conformer on its relaxed geometry in vacuum; "MD_{vac}" is the average of values calculated on the MD-derived flavin geometries with its environment excluded; "$MD_{cluster}$" corresponds to the average HFC parameters calculated on the MD-derived flavin geometries within the "minimal cluster"; and "$MD_{QM/MM}$" to the same quantity calculated with the QM/MM scheme described above. All HFC calculations were obtained using aDFT with the B3LYP functional and the mixed basis set scheme of EPR-III/GEN-A2* on the flavin's magnetic nuclei, and DZVP-GGA/GEN-A2 on the other flavin atoms and surrounding cluster. All calculations were performed in deMon2k 6.0.2.

(a) $FAD^{\bullet -}$

atom	a_{iso} (MHz)				ΔA (MHz)			
	Opt_{vac}	MD_{vac}	$MD_{cluster}$	$MD_{QM/MM}$	Opt_{vac}	MD_{vac}	$MD_{cluster}$	$MD_{QM/MM}$
N5	15.050	16.379	17.408	16.712	53.660	55.411	58.152	56.225
N10	5.916	5.931	6.828	6.882	19.418	16.586	18.830	18.767
H1'a	2.805	2.754	3.580	3.400	3.819	3.675	3.913	3.782
H1'b	6.559	5.232	5.992	6.302	3.866	3.549	3.729	3.612
H8α	12.392	10.118	10.342	9.847	2.869	2.501	2.349	2.369
H7α	-3.668	-3.461	-3.273	-3.238	1.773	1.596	1.609	1.597
H6	-10.125	-9.243	-8.064	-8.440	7.723	6.999	6.622	6.674

(b) $FADH^{\bullet}$

atom	a_{iso} (MHz)				ΔA (MHz)			
	Opt_{vac}	MD_{vac}	$MD_{cluster}$	$MD_{QM/MM}$	Opt_{vac}	MD_{vac}	$MD_{cluster}$	$MD_{QM/MM}$
N5	11.987	16.829	17.129	17.153	43.793	45.475	46.522	46.768
N10	7.209	7.499	7.855	7.568	21.492	19.752	20.741	20.129
H1'a	3.423	2.247	2.438	2.413	3.886	3.596	3.667	3.631
H1'b	7.423	14.002	14.740	13.810	3.930	3.700	3.773	3.733
H8α	7.476	5.656	6.544	6.047	1.910	1.594	1.661	1.608
H7α	-0.950	-0.901	-0.684	-1.122	1.407	1.271	1.339	1.302
H6	-4.755	-3.584	-3.285	-3.528	4.596	4.464	4.513	4.459
H5	-22.675	-18.591	-19.159	-19.366	31.631	33.211	33.822	34.008

Table 2: Principal components of the HFC tensors for atoms of **(a)** $FADH^{\bullet}$ and **(b)** $FAD^{\bullet-}$. The labels "$MD_{cluster}$" and "$MD_{QM/MM}$" refer respectively to the averaged tensors calculated for the flavin in a QM cluster and in a QM/MM protein environment; "MD_{vac}" refers to the tensors calculated on the same set of flavin geometries, but stripped from its protein environment.

(a) $FADH^{\bullet}$

atom	A_{YY}			A_{XX}			A_{ZZ}		
	MD_{vac}	$MD_{cluster}$	$MD_{QM/MM}$	MD_{vac}	$MD_{cluster}$	$MD_{QM/MM}$	MD_{vac}	$MD_{cluster}$	$MD_{QM/MM}$
N5	1.793	1.720	1.665	1.548	1.523	1.462	47.145	48.143	48.332
N10	1.058	1.076	0.997	0.771	0.807	0.720	20.667	21.682	20.988
H1'a	1.178	1.344	1.322	0.919	1.087	1.083	4.645	4.883	4.834
H1'b	13.015	13.689	12.754	12.522	13.275	12.377	16.469	17.255	16.299
H8α	5.218	6.106	5.610	5.031	5.875	5.411	6.718	7.652	7.119
H7α	-1.232	-1.025	-1.456	-1.417	-1.234	-1.656	-0.053	0.209	-0.254
H6	-4.677	-4.388	-4.635	-5.467	-5.191	-5.394	-0.608	-0.277	-0.556
H5	-23.190	-23.857	-24.172	-36.132	-37.009	-37.233	3.550	3.389	3.306

(b) $FAD^{\bullet-}$

atom	A_{YY}			A_{XX}			A_{ZZ}		
	MD_{vac}	$MD_{cluster}$	$MD_{QM/MM}$	MD_{vac}	$MD_{cluster}$	$MD_{QM/MM}$	MD_{vac}	$MD_{cluster}$	$MD_{QM/MM}$
N5	-1.922	-1.827	-1.8771	-2.261	-2.125	-2.203	53.320	56.176	54.216
N10	0.516	0.666	0.7386	0.290	0.436	0.515	16.989	19.382	19.393
H1'a	1.747	2.477	2.3442	1.311	2.074	1.934	5.204	6.189	5.921
H1'b	4.330	5.034	5.3805	3.768	4.464	4.816	7.598	8.478	8.710
H8α	9.372	9.691	9.1594	9.196	9.427	8.955	11.786	11.907	11.426
H7α	-3.843	-3.663	-3.6253	-4.143	-3.956	-3.915	-2.397	-2.200	-2.173
H6	-10.858	-9.769	-10.1102	-12.293	-10.773	-11.218	-4.577	-3.649	-3.990

On average, the absolute deviation of the absolute value of tensors components induced by the inclusion of the environment is 0.448 ± 0.937 ($MD_{cluster}$) or 0.302 ± 0.819 ($MD_{QM/MM}$) MHz for the neutral semiquinone; the largest change is $\Delta A_{zz} = +1.186 \pm 0.809$ MHz, which occurs for N5 ($MD_{QM/MM}$). For the radical anion, the average absolute deviation is more reliable, equal to 0.729 ± 0.297 ($MD_{cluster}$) or 0.614 ± 0.283 ($MD_{QM/MM}$) MHz, and the largest change is $\Delta A_{zz} = +2.856 \pm 0.659$ MHz for N5. N10 is also significantly affected, with $\Delta A_{zz} = +2.393 \pm 0.525$ MHz ($MD_{cluster}$) or $+2.404 \pm 0.471$ MHz ($MD_{QM/MM}$). The relatively large statistical uncertainty associated to the magnitude of the shift in HFC-derived values arises from the combination of uncertainties on the MD_{vac} and $MD_{cluster/QMMM}$ datasets, and makes it difficult to accurately gauge the impact of electronic polarisation on the flavin's HFC tensors.

Examination of individual HFC tensor components: To better visualize the HFC tensor components and their dependence on the protein environment, we have further studied the distributions of the projections of HFC tensors onto the averaged, normalised eigenbasis, $\mathbf{v}_{j\in\{1,2,3\}}$. Specifically, for each snapshot the projection of the hyperfine tensor $\mathbf{A}_n$ in the molecular frame (where n samples the set of $N = 400$ geometries for which HFCs were calculated) in the directions $\mathbf{v}_j$, $A_n^{(v_j)}$, was obtained by calculating $\left\|\mathbf{A}_n\mathbf{v}_j\right\|$. Histograms of these projections are reported in Figure 6 for the N5 atom, and for the N10 and H5 atoms in the SI (Figure S9). Note that only the HFC parameters for the nitrogen atoms and H5 are well representable in this way, as their symmetry gave consistent eigenvector directions across the set of diagonalised tensors. The $\mathbf{v}_3$ eigenvector corresponds to the long axis of the HFC; it aligns closely with the z-axis for the two N-atoms, and with the y-axis for H5. The so derived distributions give a more complete picture of the impact of the environment on the distributions of hyperfine interactions.

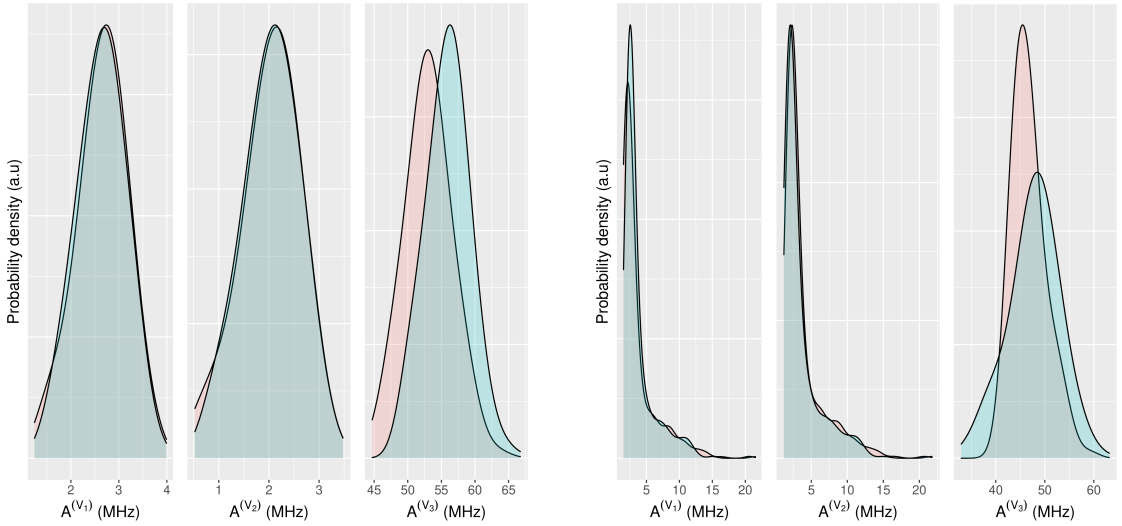

(a) $FAD^{\bullet-}$ (b) $FADH^{\bullet}$

Figure 6: Projection of the N5 HFC tensor for (a) $FAD^{\bullet-}$ and (b) $FADH^{\bullet}$ onto their average eigenvectors $\mathbf{v}_i$. Blue (resp. red) histograms refer to values calculated in $MD_{cluster}$ (resp. MD_{vacuum})

The inclusion of the environment is shown to have both a shifting and broadening effect on the distributions of $MD_{cluster}$ N5 and N10 along $\mathbf{v}_3$ i.e. on the longitudinal component $A^{(v_3)}$ of the tensors. Interestingly, while the lengthening effect applies to both protonation states, the presence of the chemical environment broadens the distributions of N5 and N10's $A^{(v_3)}$ for $FADH^{\bullet}$, but does not significantly affect the shape of the corresponding distributions in $FAD^{\bullet-}$. $A^{(v_1)}$ and $A^{(v_2)}$, i.e. the projections on the transverse axes are found to be affected for the N10 nucleus on both flavin protonation states, although to a generally weaker extent. Since these figures are included to convey qualitative insight into the effect of electronic polarisation on the distributions of HFC tensor projections, and into the shape of these distributions themselves, then only the projections from $MD_{cluster}$ tensors are reported; all

the above comments also hold true for $MD_{QM/MM}$ projections, which differ only in the details.

Graphs in Figure S5 in the SI report, respectively, the distributions of isotropic hyperfine couplings and the tensor anisotropy for the pertinent flavin atoms, calculated on the extracted geometries from the MD simulation. These quantities were again derived from the MD-extracted flavin geometries with and without its "minimal" environment, and correspond to the MD_{vac} and $MD_{cluster}$ datasets. Due to the non-normality of distributions (especially for N5 and N10), the average, quartiles, minimum and maximum of each set are reported. Average and standard deviation values for all tensor elements are also available in the SI (Section S18 and S19).

4 Discussion

We have calculated the hyperfine interactions of $FAD^{\bullet-}$ and $FADH^{\bullet}$ taking structural fluctuations and polarisation effects from the protein environment into account. Structural dynamics were accounted for by sampling molecular dynamics trajectories of 800 ns, *i.e.* a time span approaching the lifetime of radical pairs implicated with magnetoreception. Environment effects were included by a cluster approach, whereby a sensitivity analysis was used to elect the residues contributing to the cluster, allowing to model the environment on the full quantum level whilst keeping the computational demands manageable. We have observed that the hyperfine interactions are determined both by structural fluctuations, governed and confined by the protein, and by the polarising effects of the environment on the electronic structure. To gauge the relative importance of these two contributions, we shall compare the hyperfine parameters derived for the relaxed structure of the isolated radicals in vacuum, and the average values of the extracted structures, both with and without environmental effects included *via* the cluster and QM/MM model.

We will first focus the discussion on the isotropic hyperfine coupling constant and the anisotropy, as defined in the Metrics section, which are reported in Table 1 **(a,b)**. A change in a_{iso} could reflect a scaling of the whole tensor, or a change in individual principal components. The latter aspect is captured in the anisotropy, which is also the central parameter determining the directionality of the magnetic field effect for the radical pair, and which we shall discuss thereafter. It should however not be forgotten that some changes in the hyperfine parameters are undetectable by these two metrics; these can always be assessed from the complete tensors, as reported in the SI (sections 18 and 19), and from the plots of the average HFC tensors (Figure 5, **(a,b)**). Some characteristics of these will be discussed here in terms of individual tensor components and their distributions, before we comment on differences with previous HFC calculations and experimental data, as well as between our $MD_{cluster}$ and $MD_{QM/MM}$ datasets.

Isotropic HFC: Analysing the isotropic hyperfine coupling constants (Table 1), we remark the following trends: on average, the absolute change in a_{iso} due to structural fluctuation is equal to 0.9 ± 0.1 MHz for the radical anion, and 2.5 ± 0.4 MHz for the semiquinone. Electronic polarisation by the close environment, on the other hand, induces on average an absolute change of 0.7 ± 0.3 MHz ($MD_{cluster}$) or 0.6 ± 0.3 MHz ($MD_{QM/MM}$) for $FAD^{\bullet-}$, and 0.4 ± 0.9 MHz ($MD_{cluster}$) or 0.3 ± 0.8 MHz ($MD_{QM/MM}$) for $FADH^{\bullet}$. As these effects are

not necessarily additive, but may partly compensate each other, the average absolute change registered in a_{iso} upon consideration of the combined effect is about 1.3 ± 0.2 MHz ($MD_{cluster}$) or 1.2 ± 0.1 MHz ($MD_{QM/MM}$) for the anion, and 2.5 ± 0.6 MHz ($MD_{cluster}$) or 2.4 ± 0.5 MHz ($MD_{QM/MM}$) for the semiquinone.

Atoms which are particularly strongly affected by structural effects are the H8α methyl, with a deviation of about -2.3 ± 0.2 MHz, H1'b ($\Delta a_{iso} \simeq -1.3 \pm 0.2$ MHz) and N5 ($\Delta a_{iso} \simeq +1.3 \pm 0.2$ MHz) for the anion; and, even more so, H1'b ($\Delta a_{iso} \simeq +6.5 \pm 2.0$ MHz), N5 ($\Delta a_{iso} \simeq +5 \pm 0.4$ MHz) and H5 ($\Delta a_{iso} \simeq +4.6 \pm 0.8$ MHz) in the semiquinone. The inclusion of the environment seems to have a weaker impact overall, although the generally large statistical uncertainties make it difficult to conclude: the largest effects on $FAD^{\bullet -}$ atoms are deviations of $\Delta a_{iso} \simeq +1.2 \pm 0.2$, $+1.0 \pm 0.4$ and $+1.0 \pm 0.3$ MHz for H6, H1'b and N5 respectively; and $FADH^{\bullet}$ exhibits a remarkable insulation to electronic polarisation by its immediate chemical environment, with all environment-induced deviations staying below 1 MHz – the largest one occurring for H8α ($\Delta a_{iso} \simeq +0.9 \pm 0.3$ MHz).

HFC anisotropy: A similar analysis can be made for the tensor anisotropy (Table 1): on average, the absolute change in value due to structural fluctuation is equal to 0.9 ± 0.1 MHz for $FAD^{\bullet -}$ and 0.7 ± 1.1 MHz for $FADH^{\bullet}$. The average uncertainty on $FADH^{\bullet}$ ΔA is however contaminated by the very large uncertainty on the H1'b atom ($\Delta\Delta A = 6.463 \pm 5.493$ MHz), which arises because of its poor sampling in the MD_{vac} dataset: only 27 A_{zz} and 30 A_{yy} values are uncorrelated. Removing $\Delta A^{H1'b}$ from the calculation of the average deviation of anisotropy yields $\Delta\Delta A = 0.8 \pm 0.4$ MHz for $FADH^{\bullet}$. Polarisation by the cluster induces on average an absolute change of 0.8 ± 0.2 MHz ($MD_{cluster}$) or 0.5 ± 0.2 MHz ($MD_{QM/MM}$) for $FAD^{\bullet -}$, and 0.4
($MD_{cluster}$) or 0.3 ± 3.183 MHz ($MD_{QM/MM}$) for $FADH^{\bullet}$ – again contaminated by a huge uncertainty on $\Delta\Delta A^{H1'b}$. The average absolute change registered by ΔA upon addition of these two effects is about 1.0 ± 0.1 MHz ($MD_{cluster}$) or 0.8 ± 0.1 MHz ($MD_{QM/MM}$) for the anion, and 0.8 ± 2.8 MHz ($MD_{cluster}$) or 0.9 ± 2.1 MHz ($MD_{QM/MM}$) for the semiquinone.

For both protonation states of the flavin, the N10 atom is most affected by structural fluctuations: ΔA registers a decrease of 2.8 ± 0.1 MHz for the anion, and of 1.6 ± 0.1 MHz for the semiquinone. The N5 atom is the second most affected, with $\Delta\Delta A \simeq +1.8 \pm 0.1$ and $+1.6 \pm 0.6$ MHz for $FAD^{\bullet -}$ and $FADH^{\bullet}$, respectively. The subsequent polarisation by the chemical environment most strongly impacts the same two nitrogen atoms, increasing the average tensor anisotropy in $FAD^{\bullet -}$ of N5 by 2.7 ± 0.1 MHz and N10 by 2.2 ± 0.2 MHz, respectively, while increasing ΔA^{N5} by 1.3 ± 1.2 MHz in $FADH^{\bullet}$. This relatively large uncertainty again arises from poor sampling, as the $MD_{QM/MM}$ dataset contains only 57 independent A_{zz} values for N5.

In the case of N5 and N10, the HFC interactions of which are strongly axial and nearly collinear (see Figure 5), a variation in tensor anisotropy can reveal a weakening or strengthening of their axial character. Since the directional sensitivity of the magnetic compass depends on the strong axiality of this particular interactions, any change in ΔA for these atoms has implications regarding compass performance. Still, it should be noted that the variations reported here are modest: indeed, the static, vacuum picture of $FAD^{\bullet -}$ (Table 1, column "Opt_{vac}") underestimates the tensor anisotropy of N5 by about 5-8% and overestimates that of N10 by only 3%; similarly, relaxed $FADH^{\bullet}$ in vacuum underestimates ΔA by about 6%

for N5 and overestimates it by about 3-6% for N10. For both protonation states, H8α is the atom for which the relative error of the static picture is the largest, overestimating ΔA by 17-18% in $FAD^{\bullet -}$ and 12-15% in $FADH^{\bullet}$.

Individual tensor components: While tensor anisotropy reveals some information on the directionality of hyperfine couplings, a finer appreciation can be gained by comparing their eigenvalues A_{xx}, A_{yy} and A_{zz}, assigned as detailed in the Metrics section. For the strongly anisotropic atoms N5 and N10, A_{zz} is proportional to the length of the longest axis of the HFC tensor, and its direction nearly coincides with the z-axis. We note that when in a dynamic environment, N5 has significantly smaller transverse components (A_{xx} and A_{yy}, see Table 2), *i.e* by 30 to 50%, than predicted for the static flavin in vacuum (cf. Tables S6 and S7 in the SI). This has implications for the ability of the system to generate a "spike" in the orientation-dependent singlet recombination yield at long coherence times, the so-called "quantum needle" proposed to explain the remarkable angular precision of the compass: indeed, scaling down the transverse components of nitrogen tensors is expected to weaken this spike.[23] N10, on the other hand, show either a marked increase in the magnitude of its transverse components, in the case of $FADH^{\bullet}$, or a simultaneous increase of A_{yy} and decrease of A_{xx} for $FAD^{\bullet -}$, resulting in roughly interchanged values of these two components going from the static to the dynamic flavin representation.

Distributions: The distributions of selected principal tensor components are reported in Figure 6 and in the SI (Figure S9): the red and blue histogram reflect the projected tensor components including only structural fluctuations or including both structural fluctuations and polarisation effects, respectively. We notice that inclusion of the environment has both a shifting and a broadening effect on the distribution of N5 and N10 $A^{(v_3)}$, *i.e.* on the size of the tensors along their longest axis. Interestingly, while the boosting effect of the environment on the average value of A^{v_3} applies to both nitrogen tensors and protonation states of the flavin, the broadening is only apparent for the $FADH^{\bullet}$ nitrogen tensors. The reason for this shift, which arises from a different distribution of spin density on the flavin, is not attributed to the formation of a hydrogen bonds, e.g. between N5 and a nearby residue, but is a nonspecific environmental effect.

H5 is also mildly affected by the presence of the environment, registering a slight decrease in a_{iso} and increase in ΔA (Table 1). The very asymmetric distribution of a_{iso}^{H5} (Figure S5), trailing to large values, can be linked with the "out-of-planeness" of H5 with respect to the isoalloxazine rings. This is shown in the SI in Figure S10, which seeks to illuminate the relation between extreme HFC values for $FADH^{\bullet}$ H5 and geometric parameters, such as the improper angle of H5 with the isoalloxazine rings. An angle of 0° places H5 and the 3 other atoms in the same plane.

QM/MM: Average values and distributions of a_{iso} and ΔA, calculated with the QM/MM scheme described in the Results section, are reported in Figure S7 of the SI. Both the interquartile amplitude and mean values are very similar to those calculated with the "$MD_{cluster}$"

scheme. Indeed, the largest differences between these sets arise for $FAD^{\bullet-}$ N5 a_{iso} (0.7 MHz, *i.e* 4.0% change) and ΔA (1.9 MHz *i.e* 3.3% change). Considering only atoms with large and strongly anisotropic hyperfine coupling tensors (namely N5, N10, and H5), $FADH^{\bullet}$ N10 shows similarly sized relative deviation ($\Delta a_{iso} = 3.7\%$ and $\Delta\Delta A = 3.1\%$), although these changes correspond to smaller absolute value. The remaining atoms ($FAD^{\bullet-}$ N10, $FADH^{\bullet}$ N5 and H5) are on the other hand very similarly described by the QM/MM and cluster models, with deviations between their respective averaged quantities below or equal to 1.1%.

For other atoms, with smaller and/or more isotropic hyperfine coupling tensors, the relative change is contained within 0.8-7.6%, except for $FADH^{\bullet}$ H7α a_{iso} for which the cluster and QM/MM descriptions differ by 64%; however, this only corresponds to a deviation of 0.4 ± 0.2 MHz.

It is difficult to decide which approach, $MD_{cluster}$ and $MD_{QM/MM}$, best captures the effect of the electronic polarisation on flavin-borne hyperfine coupling tensors. While $MD_{QM/MM}$ includes both an accurate (*i.e* DFT-level) description of the polarising effect of the polar residues in the vicinity of the flavin, and a more rudimentary (MM) description of the rest of the protein and of the ribityl-adenosine moieties of the flavin, it also relies on a point-charge description of the backbone atoms of all neighbouring residues, which places potentially overpolarising charges close to the flavin. On the other hand, $MD_{cluster}$ treats all atoms at the DFT level, ensuring that the included chemical environment, including backbone atoms, polarises the flavin through a reasonably realistic electron density, instead of a collection of over-localised atomic charges. This gain in accuracy is balanced by the fact that the chemical environment is incomplete, limited to residues for which the election process as detailed in "Delineation of a minimal chemical environment for the flavin" indicated sizeable effects, and also lacks the ribityl-adenosine complex of the flavin. These approximations, made to keep computational demands manageable, prevent us from suggesting a hierarchy in the accuracy of results obtained from the $MD_{QM/MM}$ and $MD_{cluster}$ approaches.

Importantly, both $MD_{QM/MM}$ and $MD_{cluster}$ results suggest that the impact of polarisation on the average value of a_{iso} and ΔA is small, especially compared to that of structural fluctuations within the flavin.

Lumiflavin: The "Opt_{vac}" dataset for $FAD^{\bullet-}$, which paints a minimalist, completely static picture of the magnetic properties of the flavin, allows us to judge the suitability of the radical lumiflavin anion as approximation for cryptochrome-bound $FAD^{\bullet-}$. DFT-calculated HFCs of isolated lumiflavin have frequently been employed in the literature to support spin dynamics calculations, such as those presented in.[16,23] Structurally, the lumiflavin corresponds to the isoalloxazine moiety of the radical flavin anion, with a methyl group on the N10 atom, where the ribityl chain would start in FAD.

Considering the isotropic hyperfine couplings (Figure S6**c** in the SI), the only, but quite sizable, error ($\Delta a_{iso} \simeq 7$ MHz) arises for this methyl-group. For the flavin, the corresponding hydrogens (H1'a, H1'b) cannot be considered equivalent, as the ribityl chain prevents their equivalencing by rotation. For all other atoms however, the isotropic hyperfine couplings appear to be (surprisingly) well approximated based on the lumiflavin analogue.

The tensor anisotropy is reasonably well reproduced for N5 (Figure S6**d**, in the SI), but less so for N10. For the methyl groups (*e.g.* H8α), the reported HFCs were obtained by equating the anisotropic components to zero, as they were expected to be averaged out by the fast rotation of the methyl group. However, as can be seen from the "$MD_{cluster}$" dataset of

$FAD^{\bullet -}$, which effectively introduces this rotational averaging via sampling from the MD trajectory, some anisotropy remains. Inspecting the shapes of the averaged H8α tensors (Figure 5, right), we note this anisotropy emanates from an elongation of the HFC, along the axis of rotation and in a direction pointing towards the central ring – *i.e.* towards the center of spin density.

Experimental HFCs: Although no experimental HFCs have so far been realized for *Cl*Cry4, we can compare our results with measurements for other cryptochromes, as listed in the SI in Table 1. We note a large variability among studies, which might arise from both intrinsic differences and different experimental conditions. Data have also been reported for light oxygen voltage (LOV) domains and blue light sensor using FAD (BLUF) proteins,[42,80,81] but the cofactor (FMN instead of FAD in LOV), photo-cycle and reactivity are entirely different, suggesting that no obvious parallels can be draw beyond the distant similarity in the sense of involving a (likely) radicalized flavin cofactor.

The largest discrepancy between HFC parameters derived here and experimental results arises for the N10 atom: the $A_{\|}$ component of N10, which can be identified with A_{zz}, has been measured to be significantly larger than predicted, with experimental values ranging from 23.1 to 27.9 MHz (Table S1 in the SI) compared to $A_{zz} = 19.3$ MHz (Table 2) as derived here for $FAD^{\bullet -}$. This same discrepancy exists for $FADH^{\bullet}$. On the other hand, previous theoretical studies have found values similar to ours; and, as can be inferred from Figure S2**(b,c)** (in the SI), this particular atom does not seem to be sensitive to basis sets effects. We are therefore tempted to attribute this discrepancy to different experimental conditions (*e.g.* low temperature leading to more confinement and and sampling, different pH, etc.) or to an effect not included here, such as water binding or marked structural differences of the binding pocket compared to the crystal structure. On the other hand, such stark deviations are not expected to manifest as a result of structural fluctuations or the polarising effect of the environment alone, as our data show.

5 Conclusion

In this study, we have reported a set of hyperfine coupling tensors for the cryptochrome-bound flavin radicals derived from long-time MD and a aDFT-based cluster approaches. These average tensors, calculated on a statistically significant number of biologically relevant geometries of the flavin and its close chemical environment, are expected to provide a realistic description of the the magnetic properties of this magnetosensitive system under biologically relevant conditions. For each protonation state of the flavin considered in this paper, *i.e* the radical anion $FAD^{\bullet -}$ and the neutral radical semiquinone $FADH^{\bullet}$, we report detailed hyperfine parameters accounting for dynamic effects.

Our calculations include the structural variability of the flavin and its environment due to thermal fluctuations, and the polarisation of the electronic and spin density of the flavin by neighbouring residues. To account for the latter effect, we defined a minimal polarising cluster of amino acids, of a size suited for efficient aDFT calculations, which can be re-used in the computation of other spin-density-dependent molecular properties. This "cluster" was also

completed with the rest of the protein environment, approximated by a set of atomic point charges. The fluctuation in magnetic properties induced by these dynamical effects, which cannot be estimated from the fully static picture of a single flavin conformation in vacuum, are shown to be largely of geometrical origin, while the effect of electronic polarisation by the chemical environment is weaker. Even though the average shift of HFCs due to these dynamical effects is surprisingly small (of the order of 1 or 2 MHz for the isotropic hyperfine coupling), they induce deformations to hyperfine coupling tensors that are critical for the operation of a magnetic compass and with are expected to impact on its performance. This is e.g. the case for the induced changes of the nitrogens' A_{zz} component, or of N5's transverse components. The step-wise introduction of structural and polarising effects allowed to decorrelate and gauge their respective impact. In the same spirit, the particularly asymmetric distribution of H5's HFCs could be linked to a geometrical feature of the flavin. The new set of averaged hyperfine coupling tensors derived here for the two pertinent protonation states of the flavin radical involved in putative magnetosensitive radical pairs, will be valuable to better parametrise the spin Hamiltonian for future spin dynamics calculations. Beside average values, distributions are also reported: these could be used to inform the dynamics of HFC parameters as vital for open quantum systems spin dynamics calculations or to model the inhomogeneous distribution of hyperfine parameters expected to prevail in a biologic sample. All in all, we expect this study to help to better model the phenomenon of avian magnetoreception, and to provide a step towards elucidating its widely debated mechanisms.

6 Acknowledgments

We gladly acknowledge GENCI for generous computational resources (project number A0080706913) and the UK Defence Science and Technology Laboratory (DSTLX-1000139168) for financial support.

References

[1] R. Wiltschko and W. Wiltschko. *Magnetic orientation in animals*, volume 33. Springer Berlin Heidelberg, Berlin, Heidelberg, 1995.

[2] G. C. Nordmann, T. Hochstoeger, and D. A. Keays. Unsolved mysteries: magnetoreception-a sense without a receptor. *Plos Biol.*, 15(10):e2003234, 2017.

[3] P. J. Hore and H. Mouritsen. The radical-pair mechanism of magnetoreception. *Annu. Rev. Biophys.*, 45:299–344, 2016.

[4] K. Schulten, C. E. Swenberg, and A. Weller. A biomagnetic sensory mechanism based on magnetic field modulated coherent electron spin motion. *Z. Phys. Chem.*, 111(1):1–5, January 1978.

[5] T. Ritz, S. Adem, and K. Schulten. A model for photoreceptor-based magnetoreception in birds. *Biophys. J.*, 78(2):707–718, February 2000.

[6] R. Wiltschko, C. Nießner, and W. Wiltschko. The magnetic compass of birds: the role of cryptochrome. *Front. Physiol.*, 12:667000, May 2021.

[7] S. Y. Wong, A. Frederiksen, M. Hanić, F. Schuhmann, G. Grüning, P. J. Hore, and I. A. Solov'yov. Navigation of migratory songbirds: a quantum magnetic compass sensor. *Neuroforum*, 27(3):141–150, August 2021.

[8] A. Sancar. Structure and function of dna photolyase and cryptochrome blue-light photoreceptors. *Chem. Rev.*, 103(6):2203–2237, 2003.

[9] J. Xu, L. E. Jarocha, T. Zollitsch, M. Konowalczyk, K. B. Henbest, S. Richert, M. J. Golesworthy, J. Schmidt, V. Déjean, D. J. C. Sowood, M. Bassetto, J. Luo, J. R. Walton, J. Fleming, Y. Wei, T. L. Pitcher, G. Moise, M. Herrmann, H. Yin, H. Wu, R. Bartölke, S. J. Käsehagen, S. Horst, G. Dautaj, P. D. F. Murton, A. S. Gehrckens, Y. Chelliah, J. S. Takahashi, K.-W. Koch, S. Weber, I. A. Solov'yov, C. Xie, S. R. Mackenzie, C. R. Timmel, H. Mouritsen, and P. J. Hore. Magnetic sensitivity of cryptochrome 4 from a migratory songbird. *Nature*, 594(7864):535–540, June 2021.

[10] M. Pooam, L.-D. Arthaut, D. Burdick, J. Link, C. F. Martino, and M. Ahmad. Magnetic sensitivity mediated by the Arabidopsis blue-light receptor cryptochrome occurs during flavin reoxidation in the dark. *Planta*, 249(2):319–332, February 2019.

[11] C. Nießner, S. Denzau, L. Peichl, W. Wiltschko, and R. Wiltschko. Magnetoreception in birds: I. Immunohistochemical studies concerning the cryptochrome cycle. *J. Exp. Biol.*, 217(23):4221–4224, December 2014.

[12] R. Wiltschko, M. Ahmad, C. Nießner, D. Gehring, and W. Wiltschko. Light-dependent magnetoreception in birds: the crucial step occurs in the dark. *J. R. Soc. Interface*, 13(118):20151010, May 2016.

[13] C. Nießner, S. Denzau, L. Peichl, W. Wiltschko, and R. Wiltschko. Magnetoreception: activation of avian cryptochrome 1a in various light conditions. *J. Comp. Physiol. A*, 204(12):977–984, December 2018.

[14] P. Müller and M. Ahmad. Light-activated cryptochrome reacts with molecular oxygen to form a flavin–superoxide radical pair consistent with magnetoreception. *J. Biol. Chem.*, 286(24):21033–21040, June 2011.

[15] H. J. Hogben, O. Efimova, N. Wagner-Rundell, C. R. Timmel, and P.J. Hore. Possible involvement of superoxide and dioxygen with cryptochrome in avian magnetoreception: Origin of Zeeman resonances observed by in vivo EPR spectroscopy. *Chem.*

Phys. Lett., 480(1-3):118–122, September 2009.

[16] P. J. Hore, A. A. Lee, J. C. S. Lau, H. J. Hogben, T. Biskup, and D. R. Kattnig. Alternative radical pairs for cryptochrome-based magnetoreception. *J. R. Soc. Interface*, 11(95):20131063, 2014.

[17] C. Atkins, K. Bajpai, J. Rumball, and D. R. Kattnig. On the optimal relative orientation of radicals in the cryptochrome magnetic compass. *J. Chem. Phys.*, 151(6):065103, August 2019.

[18] N. S. Babcock and D. R. Kattnig. Radical scavenging could answer the challenge posed by electron–electron dipolar interactions in the cryptochrome compass model. *JACS Au*, 2021.

[19] N. S. Babcock and D. R. Kattnig. Electron–electron dipolar interaction poses a challenge to the radical pair mechanism of magnetoreception. *J. Phys. Chem. Lett.*, 11(7):2414–2421, April 2020.

[20] Daniel R. Kattnig. Radical-pair-based magnetoreception amplified by radical scavenging: resilience to spin relaxation. *J. Phys. Chem. B*, 121(44):10215–10227, November 2017.

[21] D. R. Kattnig and P. J. Hore. The sensitivity of a radical pair compass magnetoreceptor can be significantly amplified by radical scavengers. *Sci. Rep.*, 7(1):11640, December 2017.

[22] J. Deviers, F. Cailliez, A. de la Lande, and D. R. Kattnig. Anisotropic magnetic field effects in the re-oxidation of cryptochrome in the presence of scavenger radicals. *The Journal of Chemical Physics*, 156:025101, 1 2022.

[23] H. G. Hiscock, S. Worster, D. R. Kattnig, C. Steers, Y. Jin, D. E. Manolopoulos, H. Mouritsen, and P. J. Hore. The quantum needle of the avian magnetic compass. *Proc. Natl. Acad. Sci. U.S.A.*, 113(17):4634–4639, 2016.

[24] M. Procopio and T. Ritz. The reference-probe model for a robust and optimal radical-pair-based magnetic compass sensor. *J. Chem. Phys*, 152:65104, 2020.

[25] D. E. Manolopoulos and P. J. Hore. An improved semiclassical theory of radical pair recombination reactions. *J. Chem. Phys.*, 139(12):124106, 2013.

[26] R. K. Kar, A.-F. Miller, and M.-A. Mroginski. Understanding flavin electronic structure and spectra. *WIREs Comput. Mol. Sci.*, page e1541, 2021.

[27] Y. Ding, A. S. Kiryutin, A. V. Yurkovskaya, D. V. Sosnovsky, R. Z. Sagdeev, S. Bannister, T. Kottke, R. K. Kar, I. Schapiro, K. L. Ivanov, and J. Matysik. Nuclear spin-hyperpolarization generated in a flavoprotein under illumination: experimental field-dependence and theoretical level crossing analysis. *Scientific Reports*, 9(1):18436, 12 2019.

[28] N. Pompe, J. Chen, B. Illarionov, S. Panter, M. Fischer, A. Bacher, and S. Weber. Methyl groups matter: Photo-CIDNP characterizations of the semiquinone radicals of FMN and demethylated FMN analogs. *The Journal of Chemical Physics*, 151(23):235103, 12 2019.

[29] J. C. S. Lau, C. T. Rodgers, and P. J. Hore. Compass magnetoreception in birds arising from photo-induced radical pairs in rotationally disordered cryptochromes. *Journal of The Royal Society Interface*, 9:3329–3337, 12 2012.

[30] E. Pauwels, R. Declerck, T. Verstraelen, B. De Sterck, C. W. M. Kay, V. V. Speybroeck, and M. Waroquier. Influence of

protein environment on the electron paramagnetic resonance properties of flavoprotein radicals: A QM/MM study. *J. Phys. Chem. B*, 114(49):16655–16665, 2010.

[31] J. I. Martínez, P. J. Alonso, and M. Medina. The electronic structure of the neutral isoalloxazine semiquinone within Anabaena flavodoxin: New insights from HYSCORE experiments. *J. Magn. Reson.*, 218:153–162, May 2012.

[32] J. I. Martínez, S. Frago, I. Lans, P. J. Alonso, I. García-Rubio, and M. Medina. Spin densities in flavin analogs within a flavoprotein. *Biophys. J.*, 110(3):561–571, February 2016.

[33] M. Medina, A. Vrielink, and R. Cammack. ESR and electron nuclear double resonance characterization of the cholesterol oxidase from Brevibacterium sterolicum in its semiquinone state. *Eur. J. Biochem.*, 222:941–947, 1994.

[34] M. Medina, C. Gomez-Moreno, and R. Cammack. Electron spin resonance and electron nuclear double resonance studies of flavoproteins involved in the photosynthetic electron transport in the cyanobacterium Anabaena sp. Pcc 7119. *Eur. J. Biochem*, 227:529–536, 1995.

[35] S. Weber, G. Richter, E. Schleicher, A. Bacher, K. Möbius, and C. W.M. Kay. Substrate binding to DNA photolyase studied by electron paramagnetic resonance spectroscopy. *Biophys. J.*, 81(2):1195–1204, August 2001.

[36] E. Schleicher, K. Hitomi, C. W.M. Kay, E. D. Getzoff, T. Todo, and S. Weber. Electron nuclear double resonance differentiates complementary roles for active site histidines in (6-4) photolyase. *J. Biol. Chem.*, 282(7):4738–4747, February 2007.

[37] E. Schleicher, R. Wenzel, M. Ahmad, A. Batschauer, L.-O. Essen, K. Hitomi, E. D. Getzoff, R. Bittl, S. Weber, and A. Okafuji. The electronic state of flavoproteins: investigations with proton electron–nuclear double resonance. *Appl. Magn. Reson.*, 37(1-4):339–352, January 2010.

[38] J. I. García, M. Medina, J. Sancho, P. J. Alonso, C. Gómez-Moreno, J. A. Mayoral, and J. I. Martínez. Theoretical analysis of the electron spin density distribution of the flavin semiquinone isoalloxazine ring within model protein environments. *J. Phys. Chem. A*, 106(18):4729–4735, 2002.

[39] M. Procopio and T. Ritz. Inhomogeneous ensembles of radical pairs in chemical compasses. *Sci. Rep.*, 6(1):2045–2322, 2016.

[40] S. Weber, K. Mo, G. Richter, and C. W. M. Kay. The electronic structure of the flavin cofactor in DNA photolyase. *JACS*, 123(16):3790–3798, 2001.

[41] D. R. Kattnig, I. A. Solov'yov, and P. J. Hore. Electron spin relaxation in cryptochrome-based magnetoreception. *Phys. Chem. Chem. Phys.*, 18(18):12443–12456, 2016.

[42] D. Nohr, R. Rodriguez, S. Weber, and E. Schleicher. How can epr spectroscopy help to unravel molecular mechanisms of flavin-dependent photoreceptors? *Front. Mol. Biosci.*, 2:49, 2015.

[43] D. Nohr, S. Weber, and E. Schleicher. Epr spectroscopy on flavin radicals in flavoproteins. In Bruce A. Palfey, editor, *New Approaches for Flavin Catalysis*, volume 620 of *Methods in Enzymology*, chapter 10, pages 251–275. Academic Press, 2019.

[44] D. Nohr, S. Franz, R. Rodriguez, B. Paulus, L.-O. Essen, S. Weber, and E. Schleicher. Extended electron-transfer in animal cryptochromes mediated by a tetrad of aromatic amino acids. *Biophys. J.*, 111(2):301–311, July 2016.

[45] B. D. Zoltowski, Y. Chelliah, A. Wickramaratne, L. Jarocha, N. Karki, W. Xu, H. Mouritsen, P. J. Hore, R. E. Hibbs, C. B. Green, and J. S. Takahashi. Chemical and structural analysis of a photoactive vertebrate cryptochrome from pigeon. *Proc. Natl. Acad. Sci. U.S.A.*, 116(39):19449–19457, 2019.

[46] B. I. Dunlap, J. W. D. Connolly, and J. R. Sabin. On first-row diatomic molecules and local density models. *The Journal of Chemical Physics*, 71(12):4993, 1979.

[47] J. W. Mintmire and B. I. Dunlap. Fitting the Coulomb potential variationally in linear-combination-of-atomic-orbitals density-functional calculations. *Physical Review A*, 25(1):88–95, 1 1982.

[48] J. W. Mintmire, J. R. Sabin, and S. B. Trickey. Local-density-functional methods in two-dimensionally periodic systems. Hydrogen and beryllium monolayers. *Physical Review B*, 26(4):1743–1753, 8 1982.

[49] H. Sambe and R. H. Felton. A new computational approach to Slater's SCF– ¡i¿X¡/i¿ α equation. *The Journal of Chemical Physics*, 62(3):1122–1126, 2 1975.

[50] F. Schuhmann, D. R. Kattnig, and I. A. Solov'yov. Exploring post-activation conformational changes in pigeon cryptochrome 4. *J. Phys. Chem. B*, 125(34):9652–9659, September 2021.

[51] E. Krieger and G. Vriend. YASARA View - molecular graphics for all devices - from smartphones to workstations. *Bioinformatics*, 30(20):2981–2982, October 2014.

[52] E. Krieger, J. E. Nielsen, C. A.E.M. Spronk, and G. Vriend. Fast empirical pKa prediction by Ewald summation. *J. Mol. Graph. Model.*, 25(4):481–486, December 2006.

[53] L. Wang, L. Li, and E. Alexov. pKa predictions for proteins, RNAs, and DNAs with the Gaussian dielectric function using DelPhi pKa. *Proteins: Struct., Funct., Bioinf.*, 83(12):2186–2197, December 2015.

[54] L. Wang, M. Zhang, and E. Alexov. DelPhiPKa web server: predicting pKa of proteins, RNAs and DNAs. *Bioinformatics*, 32(4):614–615, February 2016.

[55] S. Pahari, L. Sun, S. Basu, and E. Alexov. DelPhiPKa: Including salt in the calculations and enabling polar residues to titrate. *Proteins: Struct., Funct., Bioinf.*, 86(12):1277–1283, December 2018.

[56] T. J. Dolinsky, P. Czodrowski, H. Li, J. E. Nielsen, J. H. Jensen, G. Klebe, and N. A. Baker. PDB2PQR: expanding and upgrading automated preparation of biomolecular structures for molecular simulations. *Nucleic Acids Res.*, 35(Web Server):522–525, May 2007.

[57] T. J. Dolinsky, J. E. Nielsen, J. A. McCammon, and N. A. Baker. PDB2PQR: an automated pipeline for the setup of Poisson-Boltzmann electrostatics calculations. *Nucleic Acids Res.*, 32(Web Server):665–667, July 2004.

[58] K. Sadeghian, M. Bocola, T. Merz, and M. Schütz. Theoretical Study on the Repair Mechanism of the (6-4) Photolesion by the (6-4) Photolyase. *Journal of the American Chemical Society*, 132(45):16285–16295, 11 2010.

[59] G. Lüdemann, I. A. Solov'yov, T. Kubař, and M. Elstner. Solvent Driving Force Ensures Fast Formation of a Persistent and Well-Separated Radical Pair in Plant Cryptochrome. *Journal of the American Chemical Society*, 137(3):1147–1156, 1 2015.

[60] S. Fox, H. G. Wallnoefer, T. Fox, C. S. Tautermann, and C.-K. Skylaris. First principles-based calculations of free energy of binding: application to ligand binding in

a self-assembling superstructure. *J. Chem. Theory Comput.*, 7(4):1102–1108, 2011.

[61] J.-P. Ryckaert, G. Ciccotti, and H. J. C. Berendsen. Numerical integration of the cartesian equations of motion of a system with constraints: molecular dynamics of n-alkanes. *Journal of Computational Physics*, 23(3):327–341, 3 1977.

[62] S. Miyamoto and P. A. Kollman. Settle: An analytical version of the SHAKE and RATTLE algorithm for rigid water models. *Journal of Computational Chemistry*, 13(8):952–962, 10 1992.

[63] A. M. Koster, G. Geudtner, A. Alvarez-Ibarra, P. Calaminici, M. E. Casida, J. Carmona-Espindola, V. D. Dominguez, R. Flores-Moreno, G. U. Gamboa, A. Goursot, T. Heine, A. Ipatov, A. de la Lande, F. Janetzko, J. M. del Campo, D. Mejia-Rodriguez, J. U. Reveles, J. Vasquez-Perez, A. Vela, B. Zuniga-Gutierrez, and D. R. Salahub. deMon2k, Version 6, 2018.

[64] D. Mejía-Rodríguez and A. M. Köster. Robust and efficient variational fitting of Fock exchange. *The Journal of Chemical Physics*, 141(12):124114, 9 2014.

[65] A. D. Becke. Density-functional thermochemistry. Iii. The role of exact exchange. *J. Chem. Phys.*, 98(7):5648, April 1993.

[66] P. J. Stephens, F. J. Devlin, C. F. Chabalowski, and M. J. Frisch. Ab initio calculation of vibrational absorption and circular dichroism spectra using density functional force fields. *J. Phys. Chem.*, 98(45):11623–11627, November 1994.

[67] C. Lee, W. Yang, and R. G. Parr. Development of the Colle-Salvetti correlation-energy formula into a functional of the electron density. *Phys. Rev. B*, 37(2):785, January 1988.

[68] R. Improta and V. Barone. Interplay of electronic, environmental, and vibrational effects in determining the hyperfine coupling constants of organic free radicals. *Chem. Rev.*, 104(3):1231–1254, March 2004.

[69] M. Krack and A. M. Köster. An adaptive numerical integrator for molecular integrals. *J. Chem. Phys.*, 108(8):3226, February 1998.

[70] A. de la Lande, A. Alvarez-Ibarra, K. Hasnaoui, F. Cailliez, X. Wu, T. Minerva, J. Cuny, P. Calaminici, L. López-Sosa, G. Geudtner, I. Navizet, C. Garcia Iriepa, D. R. Salahub, and A. M. Köster. Molecular Simulations with in-deMon2k QM/MM, a Tutorial-Review. *Molecules*, 24(9):1653, 4 2019.

[71] RStudio Team. *RStudio: Integrated Development Environment for R.* RStudio, PBC., Boston, MA, 2020.

[72] M. Plummer, N. Best, K. Cowles, and K. Vines. Coda: Convergence diagnosis and output analysis for mcmc. *R News*, 6(1):7–11, 2006.

[73] D. R. Roe and T. E. Cheatham. PTRAJ and CPPTRAJ: Software for Processing and Analysis of Molecular Dynamics Trajectory Data. *Journal of Chemical Theory and Computation*, 9(7):3084–3095, 7 2013.

[74] V. Barone. Structure, magnetic properties and reactivities of open-shell species from density functional and self-consistent hybrid methods. In *Recent Advances in Density Functional Methods*, volume 1, pages 287–334. World Scientific, 1995.

[75] L. Hermosilla, P. Calle, and J. M. García de la Vega. Modeling EPR parameters of nitrogen containing conjugated radical cations. *RSC Adv.*, 5(77):62551–62562, 2015.

[76] V. Barone, P. Cimino, and E. Stendardo. Development and validation of the B3LYP/N07D computational model for structural parameter and magnetic tensors of large free radicals. *J. Chem. Theory Comput.*, 4(5):751–764, May 2008.

[77] P. Jakobsen and F. Jensen. Probing basis set requirements for calculating hyperfine coupling constants. *J. Chem. Phys.*, 151(17):17407, November 2019.

[78] F Neese. The orca program system. *WIREs Computational Molecular Science*, 2:73–78, 1 2012.

[79] S. Grimme, J. G. Brandenburg, C. Bannwarth, and A. Hansen. Consistent structures and interactions by density functional theory with small atomic orbital basis sets. *The Journal of Chemical Physics*, 143:054107, 8 2015.

[80] K. S. Conrad, C. C. Manahan, and B. R. Crane. Photochemistry of flavoprotein light sensors. *Nature Chemical Biology*, 10(10):801–809, 10 2014.

[81] B. Kopka, K. Magerl, A. Savitsky, M. D. Davari, K. Röllen, M. Bocola, B. Dick, U. Schwaneberg, K.-E. Jaeger, and U. Krauss. Electron transfer pathways in a light, oxygen, voltage (LOV) protein devoid of the photoactive cysteine. *Scientific Reports*, 7(1):13346, 12 2017.